Multidiszciplináris Tudományok, 15. kötet, 2. sz. (2025) pp. 116–136. ***https://doi.org/10.35925/j.multi.2025.2.8***

INFLUENCE OF SAMPLE PREPARATION AND GEOMETRICAL DEVIATION ON THE DESTRUCTIVE TESTING OUTCOMES OF RSW JOINTS IN AHSS

Sahm Alden Abd Al Al
PhD student, Institute of Materials Science and Technology
Faculty of Mechanical Engineering and Informatics, University of Miskolc
3515 Miskolc-Egyetemváros, e-mail: sahm.alden@uni-miskolc.hu

Ákos Meilinger
associate professor, Institute of Materials Science and Technology
Faculty of Mechanical Engineering and Informatics, University of Miskolc
3515 Miskolc-Egyetemváros, e-mail: akos.meilinger@uni-miskolc.hu

Marcell Gáspár
full professor, Institute of Materials Science and Technology
Faculty of Mechanical Engineering and Informatics, University of Miskolc
3515 Miskolc-Egyetemváros, e-mail: marcell.gaspar@uni-miskolc.hu

Abstract

This study emphasizes the critical importance of sample preparation in resistance spot welding (RSW) for ensuring the integrity and reliability of the welding process, particularly when dealing with high-strength materials (dual phase DP600 and martensitic steel MS1400). By conducting a series of experiments that introduce various geometrical inaccuracies, such as misalignment and dimensional errors, the study quantifies their impact on tensile strength, displacement, and failure modes during tensile-shear and cross-tension tests. Key aspects such as spot welder calibration, surface conditions, dimensional accuracy, and alignment procedures are thoroughly examined. The investigation reveals that geometrical deviations in specimen preparation can significantly affect the mechanical properties assessment of welded joints.

Keywords: *Resistance spot welding, AHSS, sample preparation, mechanical tests*

1. Introduction

Resistance spot welding (RSW) has several benefits for the automotive sector, such as enhanced efficiency, cost-effectiveness, strong joints, low material distortion, adaptability, and environmental sustainability. The importance of RSW in vehicle production, and its capacity to help the industry fulfill high quality requirements, is highlighted by scientific study (Manladan et al., 2017; Brožek et al., 2017).

Advanced High-Strength Steel (AHSS) has exceptional strength and ductility in comparison to conventional steel, resulting in a substantial improvement in the crashworthiness of automobiles. This material enables the creation of more lightweight automobiles while maintaining safety standards. Utilizing AHSS in crucial structural elements enhances the capacity to absorb and disperse energy more efficiently in the event of collisions (Oikawa et al., 2006). *Figure 1* depicts a schematic illustration of

various grades of steel, including Ultra High Strength Steel (UHSS), utilized in the body structure of the Volvo XC90 as an exemplar.

Figure 1. *Body in white (BIW) colored schematic of Volvo XC90 (2019)* (volvocars.com)

Although welding AHSS has obstacles, current research and technical improvements persistently enhance the effectiveness and dependability of these procedures. It is essential to combine AHSS with optimal welding techniques to create the next iteration of lightweight, high-performance automobiles (Rajarajan et al., 2022; Hu et al., 2021).

Moreover, the automotive industry's transition towards lightweight and high-strength materials, aimed at enhancing fuel efficiency and minimizing emissions, has heightened the significance of RSW as a crucial procedure. To ensure the structural integrity of the vehicle, it is necessary to do thorough mechanical testing to optimize welding conditions and guarantee the quality of the welds (Nazari et al., 2022; Manladan et al., 2015).

Mechanical testing is essential for evaluating the quality and dependability of resistance spot welding (RSW) in the automobile sector. The significance of this is emphasized by the fact that a typical contemporary vehicle consists of several spot welds, which endure different static, impact, and fatigue stresses over the vehicle's lifetime. The welding conditions and materials employed have a considerable impact on the mechanical properties of spot welds, including tensile strength and failure mechanisms. Research has indicated that the size of the nugget, which plays a crucial role in determining the weld's strength, escalates as the welding current and time. Nevertheless, an excessive of welding current might result in expulsion and further defects, underscoring the necessity for meticulous regulation of welding parameters (Afshari et al., 2013; Zhao et al., 2023).

The importance of mechanical testing is heightened when considering AHSS utilized in the automotive sector. AHSS materials, chosen for their exceptional strength-to-weight ratio, present unique challenges in spot welding due to their complex microstructures and susceptibility to various failure modes. Mechanical testing enables the assessment of the mechanical properties of welds by uniaxial tensile tests, offering valuable information regarding their performance and dependability (Pittner et al., 2019).

Ensuring the reliability and integrity of test results is contingent upon the essential importance of the quality of mechanical testing sample preparation. The accuracy and reproducibility of mechanical testing conclusions are directly influenced by the physical features of the sample. Geometrical deviations

during the welding process can have a major impact on the results of specimen testing, which is essential for evaluating the quality of the weld. This impact can be analyzed through various aspects of the welding process and the testing methods used. The testing specimens' dimensions, including width and overlap, can vary considerably across various standards and codes. This variation impacts the consistency and comparability of test results. For example, the International Organization for Standardization (ISO) and the American Welding Society (AWS) have different requirements for specimen dimensions, which can lead to different interpretations of weld quality.

Variations in the position of spot welds can lead to significant geometrical variations in the final assembly of sheet metal parts. This variation affects the dimensional integrity and overall quality of the welded structure (Zhou et al., 1999).

Geometrical deviation can impact the failure characteristics of welded joints during mechanical testing. For instance, research conducted by Mathiszik et al. (2024) has demonstrated that the width of the specimen has a substantial impact on the failure behavior observed during tensile shear testing. The reason for this is that differences in the width of the specimen can change how stress is distributed and how much force the weld can handle during testing. variations in electrode geometry can influence the transport variables during welding, which in turn affects the quality and consistency of the weld (Wei et al., 2013).

The fatigue strength of spot welds is influenced by both the geometrical factors and their variability. Slight deviations in geometric parameters can have a substantial impact on the fatigue performance of welded structures, which is crucial for ensuring their long-term durability (R. Mohan Iyengar et al., 2009).

Geometrical deviation in resistance spot welding refers to the variations in the dimensions and positions of welds that occur during the welding process. These deviations can significantly impact the quality and structural integrity of the welded assemblies, particularly in precision-dependent industries like automotive manufacturing. Geometrical deviations can arise from variations in the spot weld positions, which affect the overall geometrical quality of the final assembly. For example, deviations in spot weld positions can lead to misalignments and inconsistencies in the assembly, impacting the dimensional integrity and functional performance of the product (Mali et al., 2012; Söderberg et al., 2012).

The sequence in which spot welds are applied also plays a crucial role in the final geometrical outcome. Incorrect sequencing can lead to accumulative deviations that affect the entire assembly process. For instance, in automotive body-in-white (BIW) assemblies, the initial spot welds (geometry points) are critical for setting the correct geometry before further welding. Any deviations in these initial points can propagate through subsequent welding stages, leading to significant geometrical inaccuracies in the final product (Tabar et al., 2020).

The dimensions of testing specimens play a pivotal role in the reliability of tensile-shear tests for resistance spot welded joints. Variations in specimen width, for instance, have been shown to significantly influence the failure behavior of the welds under testing conditions. A study highlighted that different standards and specifications recommend varying dimensions for tensile-shear testing specimens, which can lead to discrepancies in test results and interpretations of weld quality (Zhou et al., 1999).

This variability can affect the perceived strength and durability of the weld, potentially leading to underestimation or overestimation of its capabilities.

The quality of a spot weld is often evaluated based on the size and integrity of the weld nugget. Geometrical deviations during welding, such as misalignment of the electrode or inconsistencies in electrode force, can lead to irregularities in the nugget formation. These irregularities can complicate the measurement of nugget diameter, which is a critical parameter for assessing weld quality (Stephen et al., 2021).

Inaccuracies in these measurements can result in non-compliance with quality standards and potentially lead to welds that are weaker than required. Variations in electrode geometry, for example, affect the heat distribution during the welding process, which in turn influences the microstructure and mechanical properties of the weld (Wei et al., 2013; den Uijl et al., 2007). These changes can lead to unexpected behaviors under load, such as increased susceptibility to fatigue or reduced tensile strength, which might not be adequately predicted by standard testing protocols.

The deformation of the sheet can influence the pattern of weld nugget development. For instance, if the sheets being welded are not flat or if there is a gap due to deformation, it can lead to uneven heat distribution during the welding process. This uneven heat can result in inconsistent nugget growth, which is critical for the strength and quality of the weld (Pouranvari et al., 2011). Deformation in the sheets can affect the contact pressure between the electrodes and the sheets. Proper contact is essential for effective heat generation and current transfer during welding. Any irregularities in the sheet surface due to deformation can lead to poor contact, resulting in weak or defective welds (Moshayedi et al., 2014).

The mechanical properties such as tensile shear strength and peel tensile strength of spot-welded joints are directly influenced by the strength of the steel sheets being welded. A decrease in sheet thickness, which can be a result of deformation, leads to an increase in fatigue strength. This suggests that the deformation experienced by the sheets before or during welding can have a direct impact on the fatigue behavior of the welded joints (Tohru Okada et al., 2023).

Deformation can also affect the failure modes of spot-welded joints. Different degrees of deformation may lead to variations in the failure mode under tensile or peel loading conditions, which in turn influences the overall mechanical integrity of the weld (Al-Mukhtar et al., 2016; Tohru Okada et al., 2023).

Cleanliness is crucial for achieving high-quality resistance spot welds. Contaminants such as oils, grease, oxides, and dirt on the surfaces to be welded can act as barriers to effective heat generation and metal fusion. These contaminants increase the contact resistance, leading to inconsistent heat generation and potentially weak or defective welds. The measurement of initial contact resistance is a useful method for ensuring an acceptable level of surface cleanliness (Savage et al., 1978). Surface roughness affects the contact area between the welding electrodes and the workpieces. Ideally, surfaces should have minimal roughness to ensure uniform electrode contact, which promotes consistent heat generation and nugget formation. Uneven surfaces can lead to localized overheating or insufficient heating, resulting in weak spots within the weld (Al Naimi et al., 2015; Jo et al., 2019).

Calibration ensures that the welding parameters such as current, force, and time are accurately set according to the specifications required for different materials and thicknesses. This precision is vital because even small deviations in parameters can lead to significant differences in weld quality. Proper calibration helps maintain the consistency of these parameters, thereby ensuring uniform weld quality across multiple operations (Miller Co., 2019). Proper alignment of the electrodes is crucial for ensuring that the welding force is evenly distributed across the weldment. Electrodes Misalignment can lead to uneven application of force, which in turn affects the heat generation during the welding process. This uneven heat can cause the weld nugget to form improperly, either being too small or irregularly shaped, which compromises the strength of the weld. The Misalignment can result in a joint with reduced mechanical strength and reliability, which may not meet the required standards for certain applications, particularly in critical structures like automotive bodies or aerospace components (Yanqing Li et al., 2019). As the electrode deforms, the contact area with the workpiece increases, which can reduce the current density at the contact point. This reduction in current density can lead to insufficient heat generation, Deformed electrodes can cause uneven current distribution, leading to inconsistent weld

nugget formation. This inconsistency can result in weak spots within the weld, which are susceptible to failure under mechanical stress (Bin Wang et al., 2016; Charde et al., 2012).

We can conclude that the temperature conditions must be the same in all samples to ensure the same result The precise control of temperature through welding parameters, including the adjustment of electrode temperature can significantly influence weld nugget formation, mechanical properties, and overall weld quality.

Tensile shear and cross-tension tests are standard methods for evaluating the mechanical performance of spot welds, providing essential data on the strength and failure characteristics of welded joints. The geometry of the test samples, including the size, shape, and orientation of the weld nugget, may influence the stress distribution and failure mechanisms observed during testing. The sample geometry, particularly the length and width of the sample and the positioning of the weld nugget may affect the load distribution and the identification of shear strength. smaller or off-center weld nuggets can result in stress concentrations, premature failure, and lower measured strengths. In cross-tension testing, where the force is applied perpendicularly to the weld axis, the geometry of the sample dictates the mode and location of failure.

Optimal geometries can help ensure that the failure mode is consistent and reflective of the weld's inherent strength, rather than an artifact of geometrical deviations. due to necessitating rigorous testing through tensile shear and cross-tension methods. the geometry of the samples used in these tests plays a crucial role in accurately evaluating the weld's mechanical properties. This study investigates the importance of sample geometry in tensile shear and cross-tension testing, applied on DP600 and MS1400 steel aiming to establish guidelines for sample preparation that enhance the reliability and relevance of test outcomes.

2. Materials and method

This study conducted a series of tensile shear and cross-tension tests on spot-welded samples of SSAB Docol Dual-phase DP600 steel and martensitic MS1400 steel grades, each 1.0 mm in thickness and featuring various geometrical deviations. The chemical composition and mechanical properties of the DP600 and MS1400 steels are detailed in *Tables 1* and *2*, respectively.

Table 1

The chemical composition of the Docol DP600 and MS1400 steel (weight) (Sisodia, 2016)

C	C	Si	Mn	P	S	Nb	V	B	Fe
DP600	0.098	0.20	0.81	0.015	0.002	0.014	0.010	0.0002	rest
MS1400	0.220	0.46	2.46	0.016	0.003	0.000	0.023	0.0000	rest

Table 2

The mechanical properties of the Docol DP600 and MS1400steel (Sisodia, 2016)

Grade	Yield strength $Rp_{0.2}$ (MPa)	Tensile strength R_m (MPa)	Elongation A_{80} (%)	Hardness (HV10)
DP600	448	669	18.7	204
MS1400	1391	1496	4.5	470

The effect of geometrical deviations (displacement and misalignment) on the cross-tension and tensile shear tests was thoroughly investigated on DP600 and MS1400 steel. Each test was categorized into three groups, with each group experiencing three distinct geometrical deviations. In the cross-tension test, the first group was subject to displacement along the sliding line (S.L. disp.) within the C-T test tool, the second group faced angular misalignment (Angular mis.), and the third group encountered displacement in the spot weld (S.W. disp.) from the tension center line. The deviations for the first and third groups were 0.75 mm, 1.0 mm, and 2.0 mm, respectively, while the angular misalignment for the second group was set at 3°, 4°, and 8°, respectively. Refer to *Figures 1* and *2* for visual representation. Within each group, a sample with 0.0 geometrical deviation was meticulously prepared as a reference for comparison against the other samples. For each geometrical deviation, four samples were prepared and tested for both cross-tension and tensile-shear configurations and the results represent the average values obtained from these four measurements. *Figure 2* (on the left) and *Figure 4* illustrate the geometrical standard (0.0 geometrical deviation) for both the C-T and T-S tests.

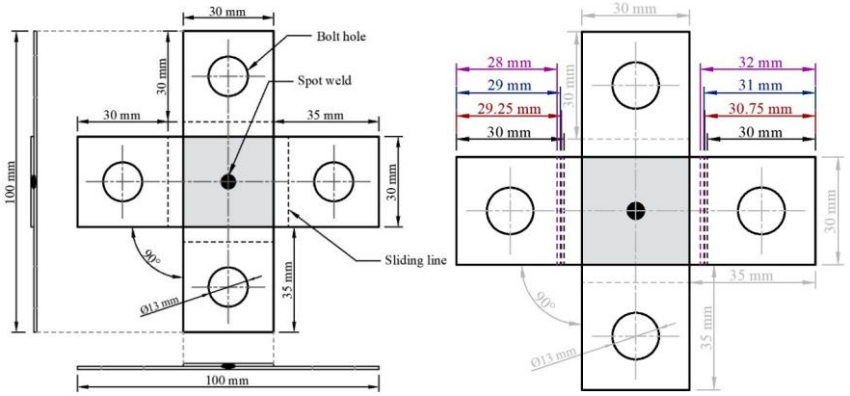

Figure 2. *Cross-tension test sample geometry drawing on the left and sliding line displacement deviation sample geometry drawing on the right*

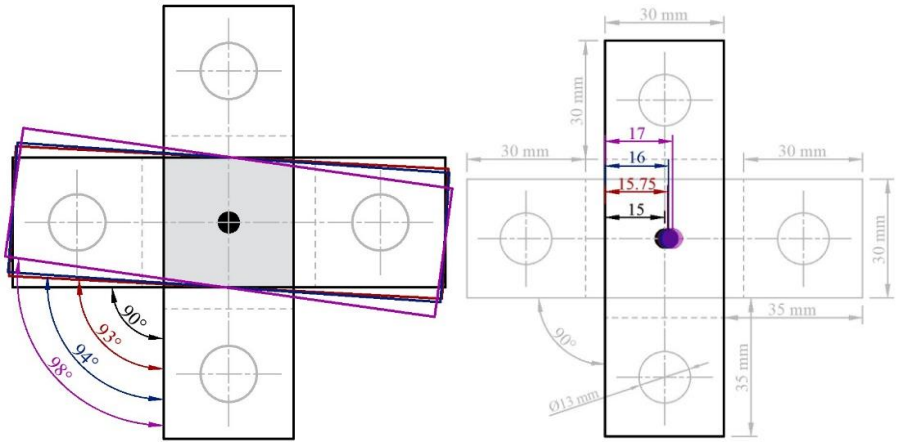

Figure 3. *C-T angular misalignment deviation sample geometry drawing on the left and spot weld displacement deviation sample geometry drawing on the right*

Regarding the tensile-shear test, it differs in the first group, the deviation is a parallel misalignment of the first sheet from the center line of the spot weld in the second sheet. Each group was compared to an accurate standard sample to determine the effect of the mentioned deviations on the test results *Figures 5, 6,* and *7* show the drawings and values of deviation in tensile-shear test groups.

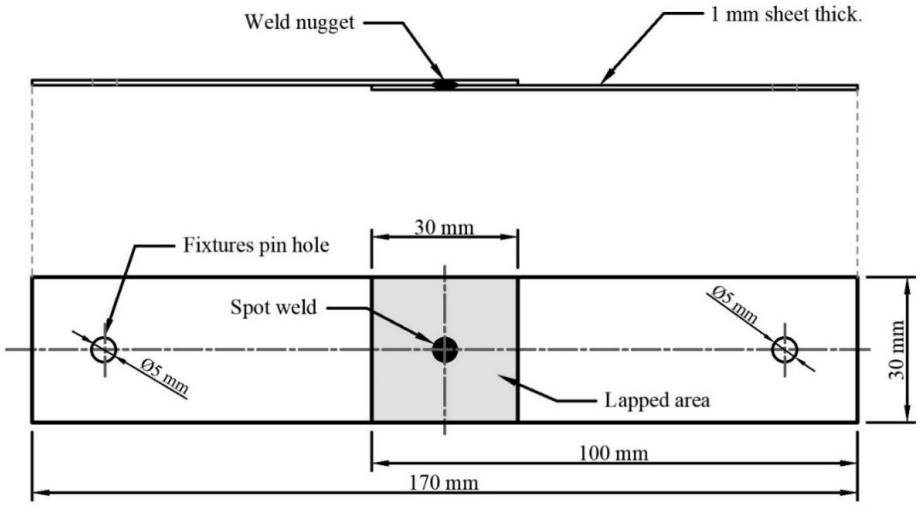

Figure 4. *Tensile-shear test sample geometry drawing*

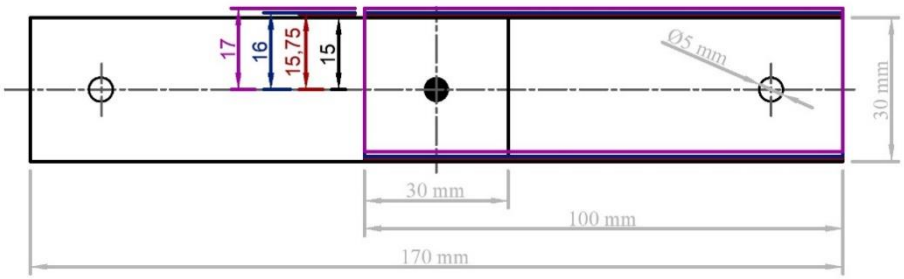

Figure 5. *Tensile-shear parallel misalignment deviation sample geometry drawing*

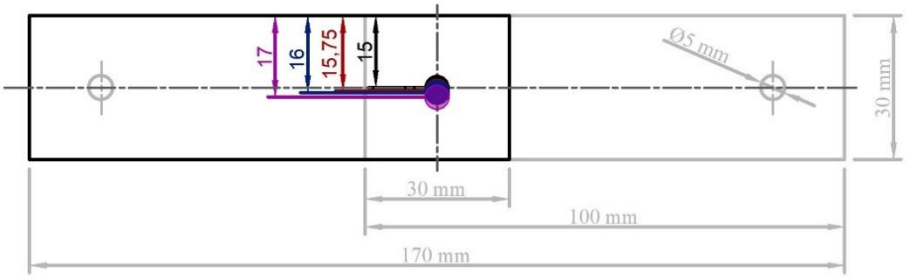

Figure 6. *Tensile-shear spot weld displacement deviation sample geometry drawing*

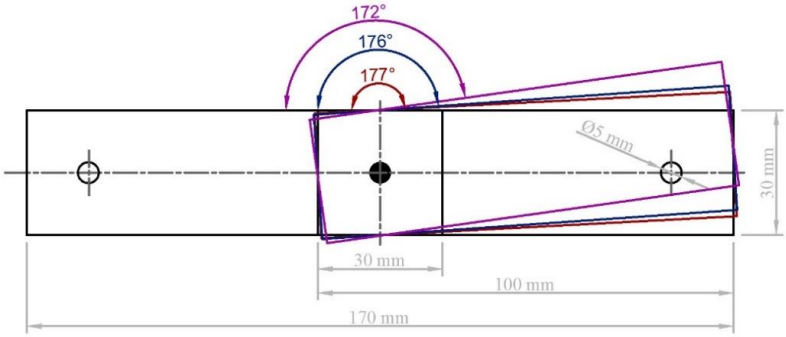

Figure 7. *Tensile-shear angular misalignment deviation sample geometry drawing*

The base metal sheets were cut to specific sizes and shapes, ensuring they were free of burrs and deformation to guarantee correct weld positioning for the test. The jigging bolt holes in the cross-tension test and the pin holes in the tensile-shear test were precisely opened, and any burrs resulting from drilling were removed using deburring tools. This is crucial because burrs can prevent testing parts from fitting together properly, leading to misalignment or assembly difficulties. All standard samples were welded within a special template to ensure there was no deviation or displacement during welding. *Figure 8* displays the template for RSW samples used in both C-T and T-S tests.

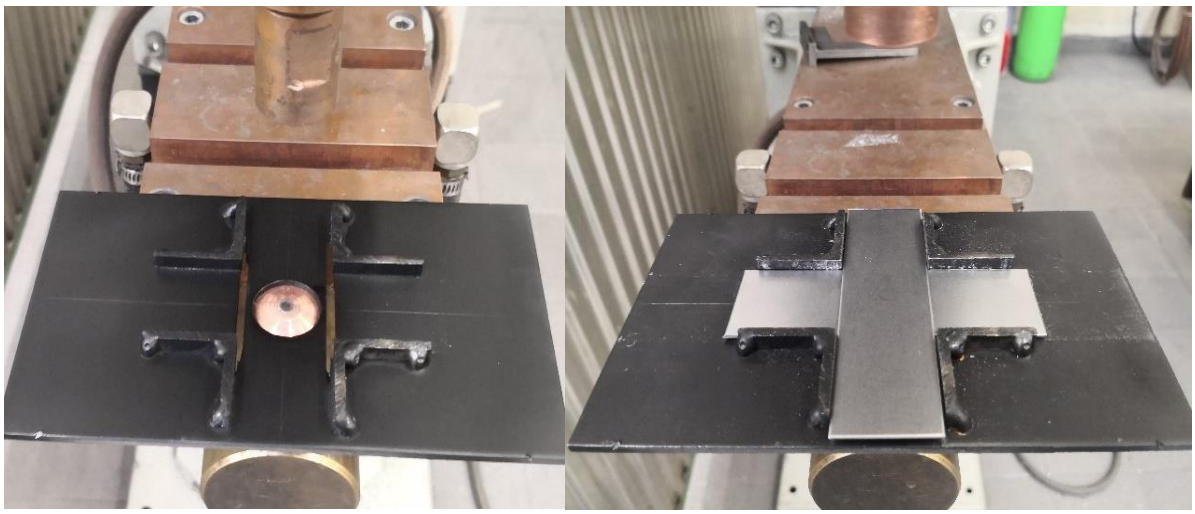

Figure 8. *Resistance spot welding samples template*

Since surface preparation is a critical step before RSW, the base metal was cleaned to remove oils, grease, oxides, and other contaminants, ensuring accurate electrical resistance across the weld interface. A dimensionally accurate cross-tension test tool was created to apply a controlled tensile force to an RSW welded joint in a cross configuration, thereby assessing its strength and performance. *Figure 9* shows a 3-D drawing of the cross-tension test tool assembly.

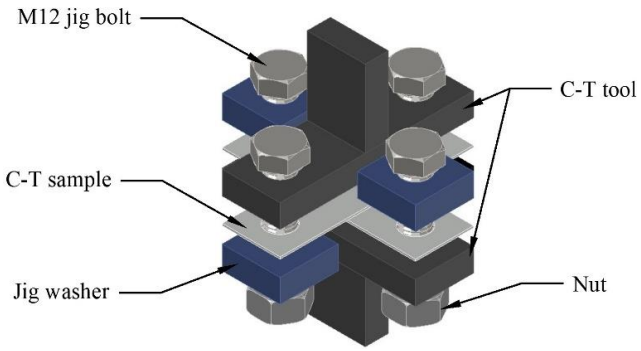

Figure 9. *3-D drawing of cross-tension test tool assembly*

RSW was performed using a projection-type TECNA 8007 spot and projection welder, operating at 50/60 Hz with an 80 kVA single-phase AC press, controlled by a TE550 microprocessor-based welding control unit. The process utilized two opposite copper chromium zirconium electrodes, turned, cut, and dressed, each with a 5 mm spherical head diameter, moving perpendicular to the sheets. The pressure (in Bar) was converted to force (in KN), applied by a pneumatic cylinder. All spot welds were conducted with the same electrode geometry and at ambient temperature. The RSW parameters for the cross-tension and tensile-shear tests applied in this study are detailed in *Table 3*.

Table 3

The mechanical properties of the Docol DP600 and MS1400steel

Base materials	Welding current [kA]	Welding time [ms]	Welding force [kN]
DP600	8.5	320	5
MS1400	8.5	320	5

Straight edges were used to verify the alignment of the electrodes, ensuring they were parallel and centered relative to each other. The calibration of resistance spot welders involved utilizing specialized instruments to measure the actual output and performance of the welding machine, with these measurements then compared against desired standards. Calibrated TECNA TE1700 RSW weld testers were employed to assess the reliability of the spot-welding machine. Various probes were connected from the tester to specific points on the welder to measure welding current, force at the electrodes, voltage at the electrodes, energy, resistance, and thermal current. *Figure 10* illustrates the probes and their functions.

Figure 10
TECNA TE1700 RSW is current measuring using a flexible transducer prob on the left and a force measuring transducer prob on the right

All RSW parameters were verified by setting specific values and then checking these using the TECNA TE1700 RSW measuring device. The input parameters closely matched the measured values, indicating that the welding machine did not require calibration. *Figure 11* presents the results of checking various welding parameters.

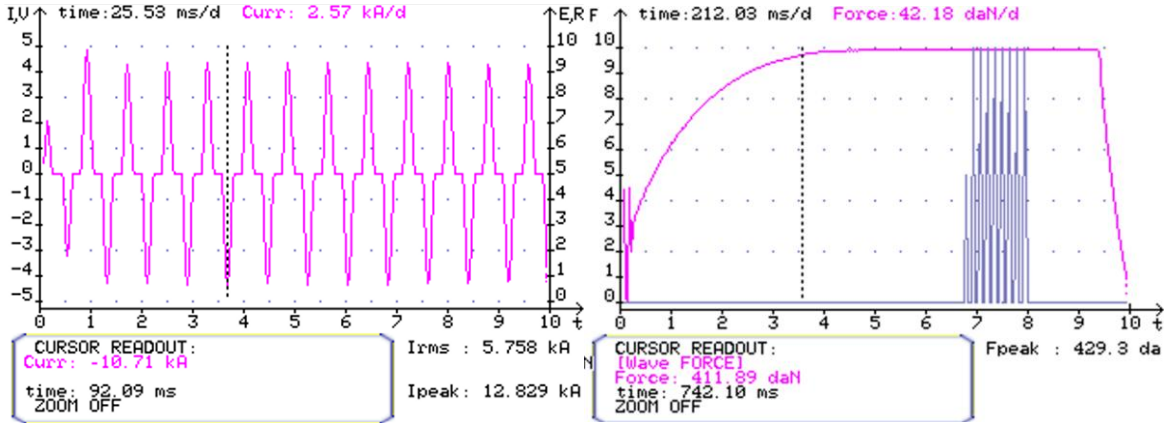

Figure 11. *Checked RSW parameters of welding force is on the left and welding current and time is on the right*

An MTS 322 test frame machine was utilized at a loading speed of 0.2 mm/s. Cross-tension appropriate grips, capable of securely holding the specific type of sample without slipping, were attached to the machine see *Figure 12*. Calibrated load cells and displacement transducers were positioned accurately. The sample was carefully placed in the testing tool, and the screws were tightened firmly to ensure proper positioning and to prevent slipping.

Figure 12. *MTS 322 test frame machine*

The samples were installed meticulously in the grips to ensure that the weld was oriented perpendicularly to the direction of the applied force and that the sample was centered and aligned properly. See *Figure 13*. A tension load was applied gradually using a hydraulically controlled mechanism until the weld failed. The data collected during the test, including the maximum force withstood, the displacement at the break, and the nature of the failure, illustrated the behavior of the sample. *Figure 14* shows the cross-tension test results of DP600 samples and *Figure 16* shows the cross-tension test results of MS1400 steel. For the tensile-shear test, two pins with a 5 mm diameter were inserted into the holes at the edges of the sample for proper grip and fixture alignment to securely hold the sample and apply force in the desired orientation. *Figure 15* shows the tensile-shear test results of DP600 steel and *Figure 17* shows the tensile-shear test results of MS1400 samples.

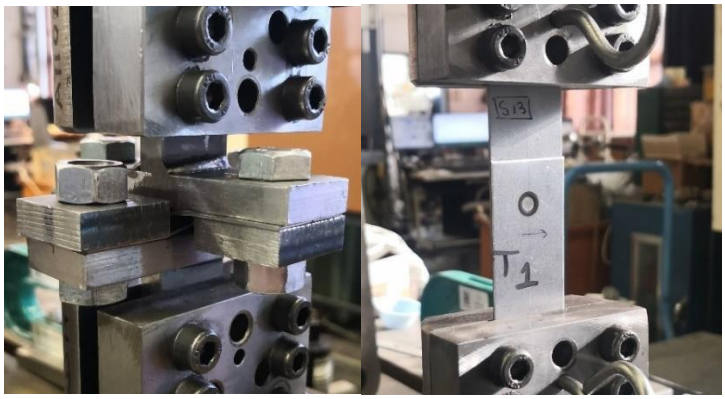

Figure 13. *Performing the C-T test on the left and the T-S test on the right*

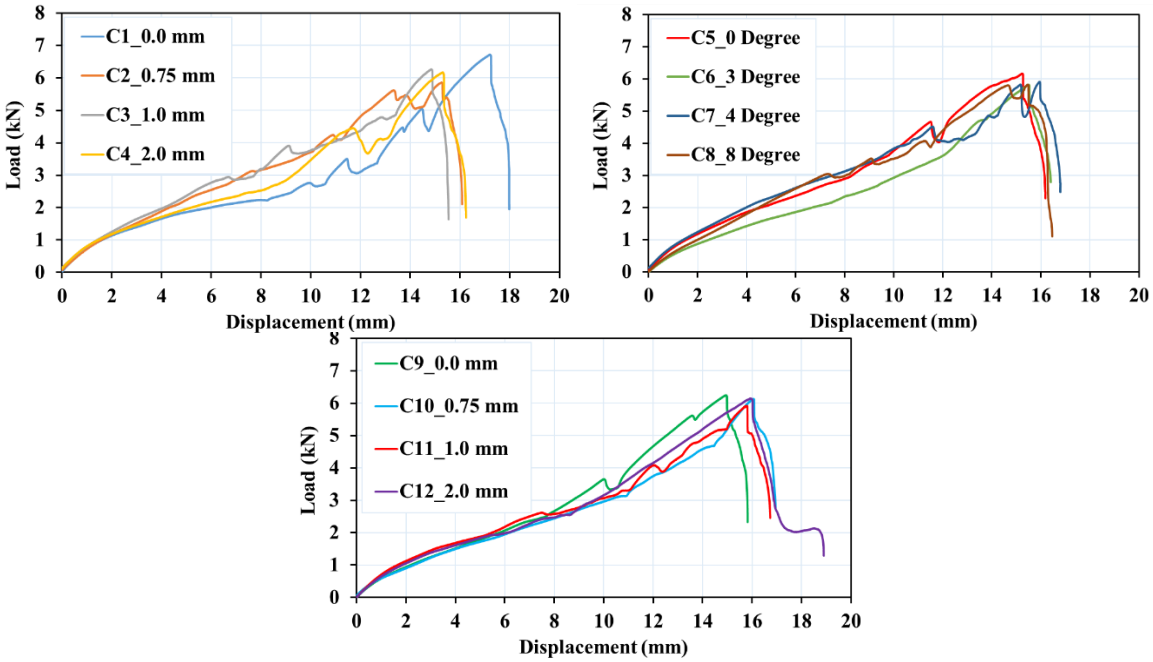

Figure 14. *DP600 cross-tension test results of all geometrical deviations*

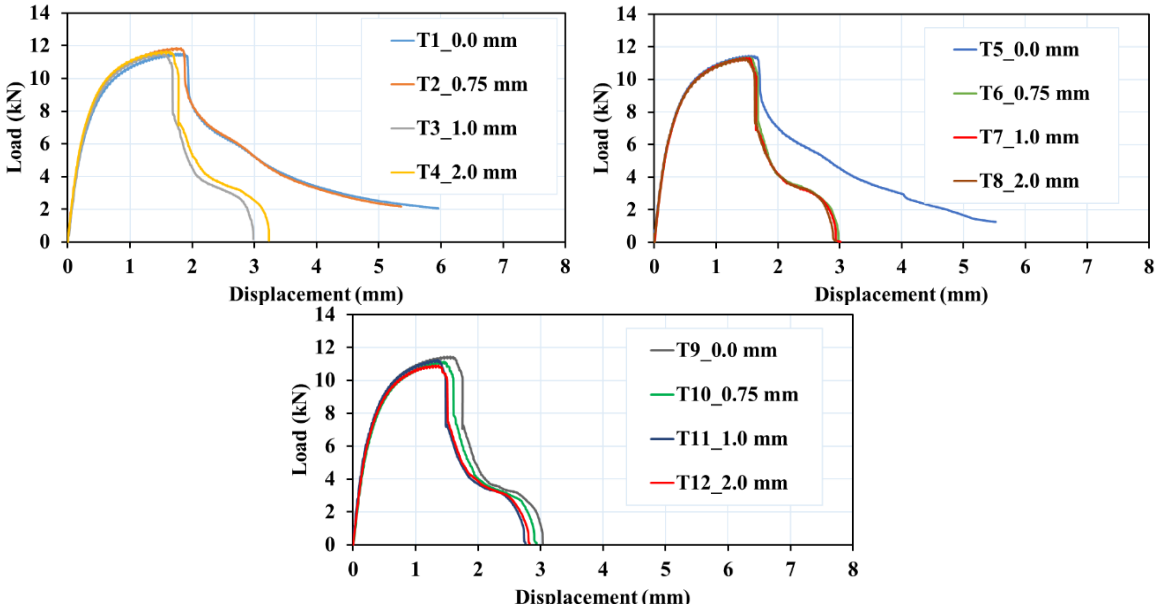

Figure 15. *DP600 tensile-shear test results of all geometrical deviations*

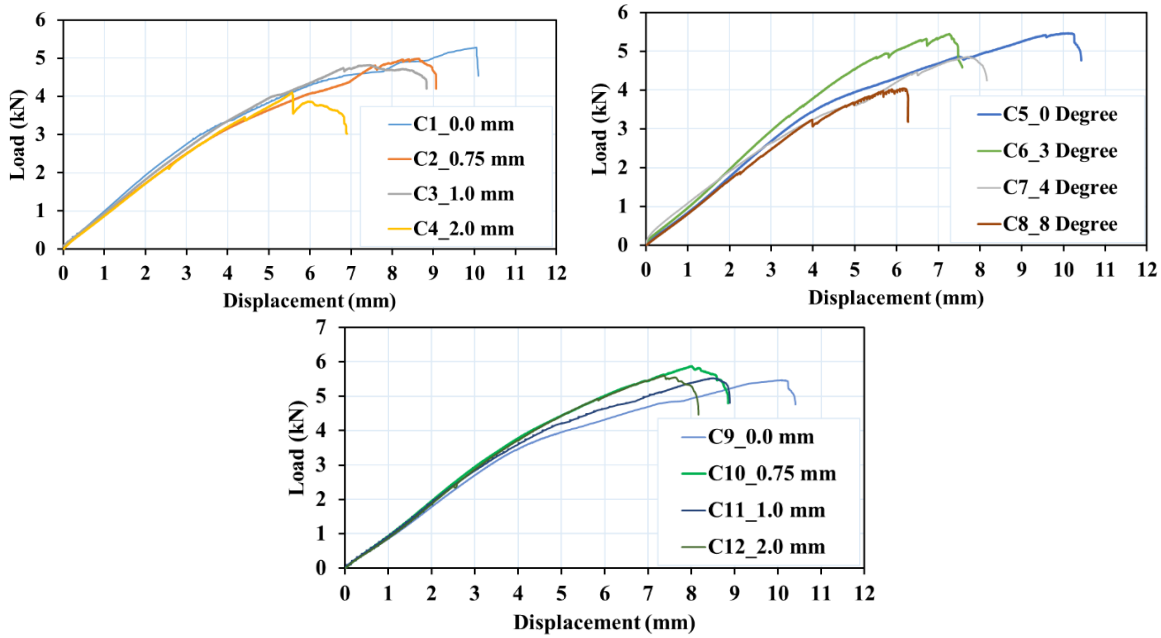

Figure 16. *MS1400 cross-tension test results of all geometrical deviations*

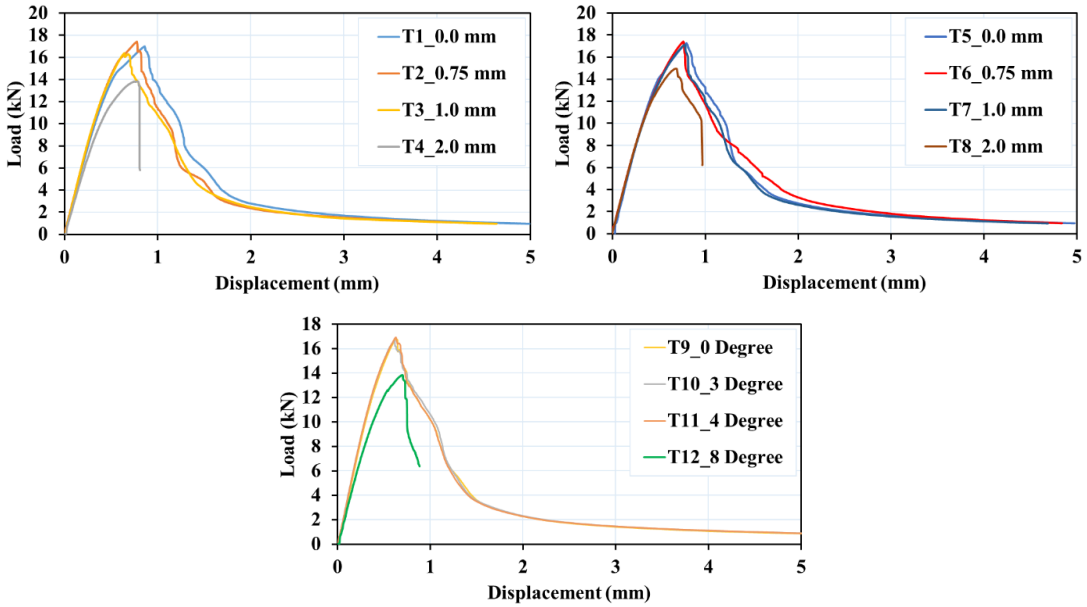

Figure 17. *MS1400 tensile-shear test results of all geometrical deviations*

3. Results and discussion

From the load-displacement figures, it is evident that there is significant convergence in the load-displacement results of the cross-tension (C-T) and tensile-shear (T-S) tests of DP600 samples. However, sample number C1 exhibited a slight superiority, see *Figures 14* and *15*. For C-T test results of MS1400 samples, it is very clear that the samples with zero deviation showed a superiority, and the samples with 2 mm and 8° degrees deviations showed a noticeable decrease compared to the standard samples, while the rest of the deviations showed a slight decrease see *Figure 16*. As for the T-S test of MS1400 steel, samples with 2 mm and 8° degrees deviations showed a significant decrease in force and a big similarity in the rest of the deviations, see *Figure 17*. In terms of the failure mode, there is also a notable similarity in the shape and size of the failures. *Tables 4, 5, 6*, and *7* display the type of deviation (Dev. Type), the value of deviation (Dev. Value), the average test load of four samples (Avg. Load), the average displacement of four samples (Avg. Disp.), and the plug diameter (dp). In our research, since the plug failure is symmetric, the plug diameter (dp) is calculated as the mean of the plug's diameters in two directions (d1, d2). *Figure 18* illustrates a schematic drawing of the symmetric plug diameter measurement.

Table 4

Cross-tension test results of DP600 samples

Sa. No.	Test Name	Dev. Type	Dev. Value	Avg. load (kN)	Avg. Disp. (mm)	Failure Mode	d1 (mm)	d2 (mm)	Avg. d1, d2 (mm)
C1	C-T	S.L disp.	0.0 mm	6.70	17.21	Plug	5.7	5.9	5.8
C2	C-T	S.L disp.	0.75 mm	5.40	15.47	Plug	5.3	5.6	5.45
C3	C-T	S.L disp.	1.0 mm	6.25	14.87	Plug	5.4	5.6	5.5

Sa. No.	Test Name	Dev. Type	Dev. Value	Avg. load (kN)	Avg. Disp. (mm)	Failure Mode	d1 (mm)	d2 (mm)	Avg. d1, d2 (mm)
C4	C-T	S.L disp.	2.0 mm	6.15	15.24	Plug	5.7	5.6	5.65
C5	C-T	Angular mis.	0° deg.	6.16	15.25	Plug	5.8	5.7	5.75
C6	C-T	Angular mis.	3° deg.	5.81	15.77	Plug	5.6	5.8	5.7
C7	C-T	Angular mis.	4° deg.	5.91	15.94	Plug	5.6	5.7	5.65
C8	C-T	Angular mis.	8° deg.	5.82	15.68	Plug	5.4	5.6	5.5
C9	C-T	S.W disp.	0.0 mm	6.24	15.21	Plug	5.6	5.7	5.65
C10	C-T	S.W disp.	0.75 mm	6.11	16.07	Plug	5.6	5.7	5.65
C11	C-T	S.W disp.	1.0 mm	5.91	15.84	Plug	5.6	5.8	5.7
C12	C-T	S.W disp.	2.0 mm	6.13	16.04	Plug	7.1	5.7	6.4

Table 5

Tensile-shear test results of DP600 samples

Sa. No.	Test Name	Dev. Type	Dev. Value	Avg. load (kN)	Avg. Disp. (mm)	Failure Mode	d1 (mm)	d2 (mm)	Avg. d1, d2 (mm)
T1	T-S	Parallel mis.	0.0 mm	11.41	1.89	PBM	NA	NA	NA
T2	T-S	Parallel mis.	0.75 mm	11.84	1.86	PBM	NA	NA	NA
T3	T-S	Parallel mis.	1.0 mm	11.50	1.55	Plug	5.4	5.1	5.25
T4	T-S	Parallel mis.	2.0 mm	11.61	1.66	Plug	5.4	5.2	5.3
T5	T-S	S.W disp.	0.0 mm	11.46	1.58	PBM	NA	NA	NA
T6	T-S	S.W disp.	0.75 mm	11.32	1.52	Plug	5.3	5.1	5.2
T7	T-S	S.W disp.	1.0 mm	11.27	1.50	Plug	5.3	5.1	5.2
T8	T-S	S.W disp.	2.0 mm	11.27	1.41	Plug	5.3	5.0	5.15
T9	T-S	Angular mis.	0° deg.	11.41	1.40	Plug	5.4	5.1	5.25
T10	T-S	Angular mis.	3° deg.	11.15	1.45	Plug	5.3	5.1	5.2
T11	T-S	Angular mis.	4° deg.	11.24	1.37	Plug	5.3	5.0	5.15
T12	T-S	Angular mis.	8° deg.	10.91	1.37	Plug	5.3	5.0	5.15

Table 6

Cross-tension test results of MS1400 samples

Sa. No.	Test	Dev. Type	Dev. Value	Avg. load (kN)	Avg. Disp. (mm)	Failure Mode	d1 (mm)	d2 (mm)	d, d3 (mm)	dp (mm)
C1	C-T	S.L disp.	0.0 mm	5.20	10.09	Plug	7.9	7.9	7.9	7.9
C2	C-T	S.L disp.	0.75 mm	4.95	9.10	P. Plug	8.0	8.1	6.28	7.19
C3	C-T	S.L disp.	1.0 mm	4.40	8.83	P. Plug	8.0	8.0	6.0	7.0
C4	C-T	S.L disp.	2.0 mm	4.10	5.70	P. Plug	7.9	7.8	5.3	6.55
C5	C-T	Angular mis.	0° deg.	5.46	10.42	Plug	7.9	7.9	7.9	7.9
C6	C-T	Angular mis.	3° deg.	5.42	7.40	P. Plug	8.0	8.0	6.7	7.35
C7	C-T	Angular mis.	4° deg.	4.81	7.39	P. Plug	8.0	7.9	7.0	7.45
C8	C-T	Angular mis.	8° deg.	4.03	6.03	P. Plug	6.1	7.3	6.3	6.8
C9	C-T	S.W disp.	0.0 mm	5.24	10.20	Plug	7.8	7.8	7.8	7.8
C10	C-T	S.W disp.	0.75 mm	5.86	8.90	P. Plug	8.1	8.1	7.1	7.6
C11	C-T	S.W disp.	1.0 mm	5.55	8.20	P. Plug	8.0	7.8	6.9	7.35
C12	C-T	S.W disp.	2.0 mm	5.01	8.86	P. Plug	7.8	7.8	6.8	7.3

Table 7

Tensile-shear test results

Sa. No.	Test	Dev. Type	Dev. Value	Avg. load (kN)	Avg. Disp. (mm)	Failure Mode	d1 (mm)	d2 (mm)	d, d3 (mm)	dp (mm)
T1	T-S	Parallel mis.	0.0 mm	17.01	0.85	Plug	7.8	7.8	7.8	7.8
T2	T-S	Parallel mis.	0.75 mm	17.40	0.78	Plug	7.8	7.8	7.8	7.8
T3	T-S	Parallel mis.	1.0 mm	16.30	0.62	Plug	7.9	7.9	7.9	7.9
T4	T-S	Parallel mis.	2.0 mm	13.30	0.79	P. Plug	7.6	7.5	5.4	6.5
T5	T-S	S.W disp.	0.0 mm	17.28	0.64	Plug	7.9	7.9	7.9	7.9
T6	T-S	S.W disp.	0.75 mm	17.11	0.78	Plug	7.9	7.9	7.9	7.9
T7	T-S	S.W disp.	1.0 mm	17.27	0.81	Plug	7.9	7.9	7.9	7.9
T8	T-S	S.W disp.	2.0 mm	14.98	0.68	Plug	7.8	7.8	7.8	7.8
T9	T-S	Angular mis.	0° deg.	17.47	0.67	Plug	7.8	7.8	7.8	7.8
T10	T-S	Angular mis.	3° deg.	16.95	0.63	Plug	7.8	7.8	7.8	7.8
T11	T-S	Angular mis.	4° deg.	16.70	0.63	Plug	7.8	7.8	7.8	7.8
T12	T-S	Angular mis.	8° deg.	13.85	0.68	Plug	7.8	7.8	7.8	7.8

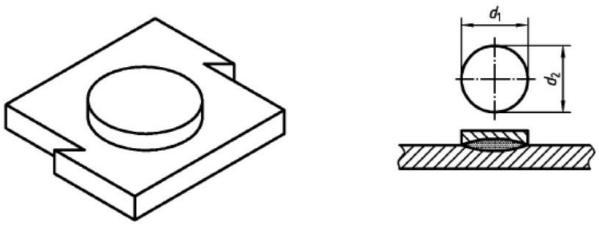

Figure 18. *Schematic drawing of the symmetric plug diameter measurement (EN ISO 14272:2001)*

In the cross-tension (C-T) test of DP600 samples, all samples exhibited a symmetrical plug failure mode within the nugget boundary, except sample C12. This sample demonstrated a combined failure mode of the plug at the nugget boundary and a bump from the heat-affected zone. *Figure 19* shows that the bump formed after the collapse, as depicted in *Figure 14*, indicating that it did not influence the outcome of the test, as detailed in *Table 4*.

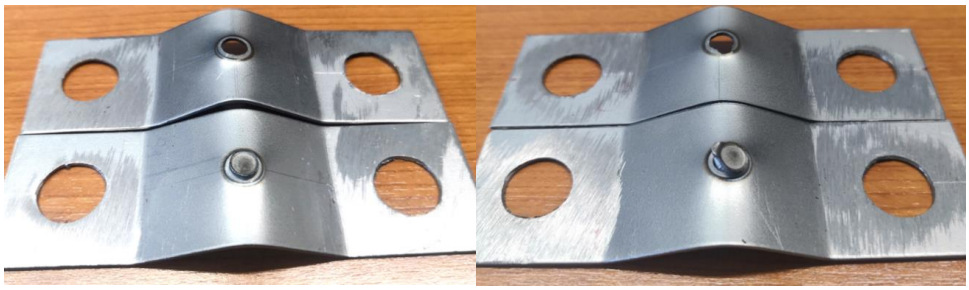

Figure 19. *Plug failure mode in sample C1 is on the left and Plug failure mode in sample C12 is on the right in DP600 samples*

In the tensile-shear (T-S) test of DP600 samples, all samples exhibited failure, predominantly through the plug failure mode, except for samples T1, T2, and T5, which failed in the plug-in base metal (PBM) mode. As depicted in *Figure 15*, these exceptions did not influence the overall results of the test. *Figures 19* and *20* showcase all types of failure modes encountered in our research.

It was observed that the failure mode occurred at the crest of the deformation in all samples. This phenomenon may result from how the metal's ductility responds to the direction of stresses during the test, contributing to the great similarity in results across samples. This principle also extends to the tensile-shear (T-S) test, where the metal's ductility may counteract the deformation, leading to uniform stresses on the spot weld and thus similar results across all tested samples.

Figure 20. *The failure mode in sample T1(plug-in base metal) is on the left and the failure mode in sample T3 (Plug) is on the right in DP600 samples*

In the cross-tension (C-T) test of MS1400 samples, C1, C5, and C9 exhibited a symmetrical circular plug failure mode within the nugget boundary see *Figure 21*. As for the failure mode in the rest of the samples, it was a partial plugin deferent sizes and patterns. *Figure 22* shows the partial plug failure mode in sample C11 of MS1400 samples, as detailed in *Table 6*.

Figure 21. *Plug failure mode in sample C1 of MS1400 samples*

Figure 22. *Partial plug failure mode in sample C11 of MS1400 samples*

In the T-S test of MS1400, the failure mode in all samples was a plug, with great similarity in size and symmetry, as shown in *Figure 23*, and all samples that had an expulsion occurred as a result of the base metal curve during welding were repeated due to unaccepted results see *Figure 24*. The expulsion is due to the base metal arcing resistance of the welding electrodes, which reduces the welding force, resulting in increases in the heat generated.

Figure 23. *Plug failure mode in sample T10 of MS1400 samples*

Figure 24. *Expulsion failure mode in testing trials of MS1400 samples*

By applying the same tests under identical conditions to ultra-high-strength steel like MS1400 and due to its high hardness and strength, this type of metal does not respond as readily to the direction of deformation in samples with geometrical deviations, resulting in uneven stresses that impact the test results compared to standard samples of the same metal. A current literature review reveals limited direct information on the effect of misalignment in cross-tension and tensile shear samples, specifically in the context of resistance spot welding RSW of any steel type. Through comparative analysis of various steel grades, it is possible to elucidate how dimensions and shapes influence stress distribution, failure modes, and overall test results. This approach provides valuable insights for optimizing sample design to accurately assess weld quality.

4. Conclusion

In this research, resistance spot welded joints on DP600 and MS1400 steel samples were subjected to cross-tension (C-T) and tensile-shear (T-S) tests with three different geometrical deviations. The investigation into the welded joints' strength and failure mode allows us to draw the following conclusions:

1. The deviations (misalignment and displacement) did not significantly affect the outcomes of the C-T and T-S tests of DP600 samples. This outcome may be attributed to the ductility of the base metal and softening in the heat-affected zone (HAZ), suggesting that fractography is essential for interpreting the destructive test results.
2. The remarkable similarity in the failure modes and test results across the samples of DP600 and MS1400 indicates that all samples were welded under consistent conditions, highlighting the crucial role of optimizing sample preparation in controlling spot welding quality.
3. In the cross-tension test, the failure mode was predominantly at the peak of the deformation and was almost symmetrical, reflecting the ductility of DP600 steel's response to spot weld strength.
4. For C-T and T-S test results of MS1400 samples, the standard samples with zero deviation showed a superiority, while the samples with 2 mm and 8° degrees deviations showed a noticeable drop proving that the higher strength of steel is more likely to be affected by the geometrical deviation.
5. The calibration of resistance spot welders is crucial to achieving high-quality welds, affecting everything from electrical control to mechanical displacement and, ultimately, the integrity of the weld.
6. The presence of metal surface contaminants, including oxides, significantly impacts the quality of resistance spot welds.

Lastly, optimizing sample preparation for destructive testing in resistance spot welding is a comprehensive process that involves precise control over welding parameters and meticulous sample preparation. These steps are vital for preserving the structural integrity of welded joints and ensuring the final product's safety and reliability.

References

[1] Manladan, S. M., Yusof, F., Ramesh, S., Fadzil, M., Luo, Z., Ao, S. (2017). A review on resistance spot welding of aluminum alloys. *The International Journal of Advanced Manufacturing Technology*, 90, 605–634. **https://doi.org/10.1007/s00170-016-9225-9**

[2] Brožek, M., Nováková, A., Niedermeier, O. (2017). Resistance spot welding of steel sheets of the same and different thickness. *Acta Universitatis Agriculturae et Silviculturae Mendelianae Brunensis*, 65 (3). **https://doi.org/10.11118/actaun2 01765030807**

[3] Oikawa, H. A., Murayama, G., Sakiyama, T., Takahashi, Y., Ishikawa, T. (2006). Resistance spot weldability of high strength steel (HSS) sheets for automobile. *Shinnittetsu Giho*, 385, 36.

[4] Information on https://www.media.volvocars.com/global/en-gb/media/photos/148215/volvo-xc90-body-structure.

[5] Rajarajan, C., Sivaraj, P., Sonar, T., Raja, S., Mathiazhagan, N. (2022). Resistance spot welding of advanced high strength steel for fabrication of thin-walled automotive structural frames. *Forces in Mechanics*, 7, 100084. **https://doi.org/10.1016/j.finmec.2022.100084**

[6] Hu, X., Feng, Z. (2021). *Advanced high-strength steel-basics and applications in the automotive industry* (No. ORNL/TM-2021/2047). Oak Ridge National Laboratory (ORNL), Oak Ridge, TN (United States). **https://doi.org/10.2172/1813170**

[7] Nazari, A. R., Talebi, A. R., Atapour, M. (2022). Resistance spot welding of advanced steels in automotive industry. In: *Proceedings of 4th International Conference and Non Destructive Testing (ICWNDT 2022)*, 1–13.

[8] Manladan, S. M., Abdullahi, I., Hamza, M. F. (2015). A review on the application of resistance spot welding of automotive sheets. *J. Eng. Technol.*, 10 (20–37), 22.

[9] Afshari, D. (2013). *Mechanical properties of resistance spot welds in lightweight applications*. Doctoral dissertation. Stockholm: KTH Royal Institute of Technology.

[10] Zhao, L., Lu, Y., Xiong, Z., Sun, L., Qi, J., Yuan, X., Peng, J. (2023). Mechanical properties and nugget evolution in resistance spot welding of Zn–Al–Mg galvanized DC51D steel. *High Temperature Materials and Processes*, 42 (1), 20220243. **https://doi.org/10.1515/htmp-2022-0243**

[11] Javaheri, E., Pittner, A., Graf, B., Rethmeier, M. (2019). Mechanical properties characterization of resistance spot welded DP1000 steel under uniaxial tensile tests. *Materials Testing*, 61 (6), 527–532. **https://doi.org/10.3139/120.111349**

[12] Zhou, M., Hu, S. J., Zhang, H. (1999). Critical specimen sizes for tensile-shear testing of steel sheets. *Welding Journal*, 78, 305-s.

[13] Mathiszik, C., Koal, J., Zschetzsche, J., Füssel, U., Schmale, H. C. (2024). Study on precise weld diameter validations by comparing destructive testing methods in resistance spot welding. *Welding in the World*, 1–11. **https://doi.org/10.1007/s40194-024-01747-z**

[14] Wei, P. S., Wu, T. H. (2013). Numerical study of electrode geometry effects on resistance spot welding. *Science and Technology of Welding and Joining*, 18 (8), 661–670. **https://doi.org/10.1179/174329313X13759662488396**

[15] Iyengar, R. M., Laxman, S., Amaya, M., Citrin, K., Bonnen, J., Kang, H. T., ... Shih, H. S. (2009). Influence of geometric parameters and their variability on fatigue resistance of spot-weld joints. *SAE International Journal of Materials and Manufacturing*, 1 (1), 299–316. **https://doi.org/10.4271/2008-01-0698**

[16] Mali, M. P., Inamdar, K. H. (2012). Effect of spot weld position variation on quality of Automobile sheet metal parts. *Int. J. Appl. Res. Mech. Eng.*, 2, 23–27.

[17] Söderberg, R., Wärmefjord, K., Lindkvist, L., Berlin, R. (2012). The influence of spot weld position variation on geometrical quality. *CIRP Annals*, 61 (1), 13–16. **https://doi.org/10.1016/j.cirp.2012.03.127**

[18] Tabar, R. S., Wärmefjord, K., Söderberg, R. (2020). A new surrogate model–based method for individualized spot welding sequence optimization with respect to geometrical quality. *The International Journal of Advanced Manufacturing Technology*, 106 (5), 2333–2346. **https://doi.org/10.1007/s00170-019-04706-x**

[19] Stephen, J. (2021). *Spot Weld Examination using NDE Methods*. Engineering Quality Inspection Services, Chennai-600095.

[20] den Uijl, N., Smith, S. (2007). The Influence of electrode geometry on resistance spot welding of advanced high strength steels for automotive applications. In: *Proceedings of 3rd JOIN Conference-International Conference on Total Welding Management in Industrial Applications*, 21–24.

[21] Pouranvari, M., Marashi, S. P. H. (2011). Critical sheet thickness for weld nugget growth during resistance spot welding of three-steel sheets. *Science and Technology of Welding and Joining*, 16 (2), 162–165. **https://doi.org/10.1179/1362171810Y.0000000016**

[22] Moshayedi, H., Sattari-Far, I. (2014). Resistance spot welding and the effects of welding time and current on residual stresses. *Journal of Materials Processing Technology*, 214 (11), 2545–2552. **https://doi.org/10.1016/j.jmatprotec.2014.05.008**

[23] Okada, T., Ueda, H., Matsuda, K., Miyazaki, Y., Yasuyama, M., Fujii, H. (2023). Effect of strength of steel sheets on tensile shear strength and failure mode of dissimilar joint of spot welds. *Welding International*, 37 (5), 282–294. **https://doi.org/10.1080/09507116.2023.2202949**

[24] Al-Mukhtar, A. M. (2016). Review of resistance spot welding sheets: processes and failure mode. *Advanced Engineering Forum*, Vol. 17, 31–57. **https://doi.org/10.4028/www.scientific.net/AEF.17.31**

[25] Savage, W. F., Nippes, E. F., Wassell, F. A. (1978). Dynamic contact resistance of series spot welds. *Welding Journal*, 57 (2), 43s–50s.

[26] Al Naimi, I. K., Al Saadi, M. H., Daws, K. M., Bay, N. (2015). Influence of surface pretreatment in resistance spot welding of aluminum AA1050. *Production & Manufacturing Research*, 3 (1), 185–200. **https://doi.org/10.1080/21693277.2015.1030795**

[27] Jo, H., Kim, D., Kang, M., Park, J., Kim, Y. M. (2019). Effects of surface roughness and force of electrode on resistance spot weldability of aluminum 6061 alloy. *Applied Sciences*, 9 (19), 3958. **https://doi.org/10.3390/app9193958**

[28] Miller Inc. (2012). *Processes Description Resistance Spot Welding*. Guidelines for Resistance Spot Welding. https://www.millerwelds.com/

[29] Li, Y., Tang, G., Ma, Y., Shuangyu, L., Ren, T. (2019). An electrode misalignment inspection system for resistance spot welding based on image processing technology. *Measur. Sci. Technol.*, 30, 075401. **https://doi.org/10.1088/1361-6501/ab1245**

[30] Wang, B., Hua, L., Wang, X., Song, Y., Liu, Y. (2016). Effects of electrode tip morphology on resistance spot welding quality of DP590 dual-phase steel. *The International Journal of Advanced Manufacturing Technology*, 83, 1917–1926. **https://doi.org/10.1007/s00170-015-7703-0**

[31] Charde, N. (2012). Effects of Eelectrode deformation on carbon steel weld geometry of resistance spot welding. *Original Research Journal*, 1 (5), 5–12.

[32] Sisodia, R. P. S. (2021). *High energy beam welding of advanced high strength steels*. PhD Dissertation. AA6 Appendix.

[33] EN ISO 14272. (2001). *Resistance welding – Destructive testing of welds – Specimen dimensions and procedure for cross tension testing of resistance spot and projection welds*.